DANMARKS OG GRØNLANDS GEOLOGISKE UNDERSØGELSE RAPPORT 2009/24

Ice sheet surface and basal topography from radar and lidar, West Greenland

Ruth H. Mottram, Susanne Hanson, Steen Savstrup Kristensen,
Andreas P. Ahlstrøm, Sine M. Hvidegaard, Henriette Skourup,
Louise Sandbjerg Sørensen, Erik Lintz Christensen,
Jens Emil Nielsen & Lars Stenseng

GEUS

DANMARKS OG GRØNLANDS GEOLOGISKE UNDERSØGELSE RAPPORT 2009/24

Ice sheet surface and basal topography from radar and lidar, West Greenland

Property of Alcoa Inc.

Ruth H. Mottram[1], Susanne Hanson[2], Steen Savstrup Kristensen[2], Andreas P. Ahlstrøm[1], Sine M. Hvidegaard[2], Henriette Skourup[2], Louise Sandbjerg Sørensen[2], Erik Lintz Christensen[2], Jens Emil Nielsen[2] & Lars Stenseng[2]

[1] Geological Survey of Denmark and Greenland, GEUS
[2] National Space Institute, Technical University of Denmark

Released 01.06.2019

GEOLOGICAL SURVEY OF DENMARK AND GREENLAND
MINISTRY OF CLIMATE END ENERGY

GEUS

Contents

Summary

This technical report presents results of a combined radar and lidar (light detection and ranging) survey carried out in West Greenland to assist the planning and development of a proposed hydropower project by Alcoa.

We discuss the techniques used to gather elevation data, describe the post-processing and spatial interpolation methods and present two digital elevation models. The first shows the surface topography derived from lidar data, the second infers the basal topography underneath the ice, based on radar data. The two are used to create a third map of ice thickness. All three models are gridded at 2 km resolution using specifically developed kriging algorithms to interpolate between the measured data points.

The gridded datasets were delivered to Alcoa on 27th February, 2009.

1. Introduction

This report presents the results of a study which used radar and lidar data to construct Digital Elevation Models (DEMs) of a glaciated part of West Greenland. The stages in the study can be summarized as

- Airborne radar and lidar survey
- Post-processing of raw data
- Development of kriging algorithms to interpolate measured topography
- Application of kriging techniques to construct maps of surface and basal topography and ice thickness

The area of interest is shown in Figure 1 below. Broadly speaking, it covers the part of Greenland that lies between 64º45'N and 66º30'N and 49º30'W to 52º00'W. The area includes part of the Greenland Ice Sheet and a small subsidiary ice cap, which although close to the ice sheet, is probably best understood as a separate glacier centre. The satellite image in Figure 3 shows that much of the area of the ice sheet is well into the ablation zone, with large lakes and individual drainage channels clearly visible. Snow obscures some of the ice surface from view.

2. Data acquisition and processing

The airborne survey was carried out during early fall 2008. This time of the year the area is dominated by repeatedly incoming low pressure systems which was also the case during the field period. To optimise the bedrock detection with the radar a low flight altitude is preferred, i.e. about 1,000 ft, and down to 500 ft in very rough areas. Furthermore, the laser scanner can not penetrate clouds, and thus the area has to be clear of clouds. During the 3 weeks of the campaign, only 8 days had good enough conditions for flying.

The area of interest covering approximately 10,000 km^2 was surveyed along parallel tracks with 2 km spacing, and in the westernmost area down to 1.5 km spacing. To calibrate the data, additional flight tracks crossing all the lines has been measured at least once (see map of flight tracks in Figure 1). The laser scanner was calibrated by various over-flights of a building in Kangerlussuaq, which position is known with very high precision. In addition an over-flight of the runway in Kangerlussuaq was performed to correlate the surfaces of the radar and laser scanner.

2.1 Instruments

A Riegl LMS-Q140i-60 near infrared laser scanner and the DTU-developed 60 MHz ice-sounder was flown on a DeHavilland DHC-6 Twin Otter registered under OY-POF chartered from Air Greenland. The ice-sounder uses radio pulses to measure the distance between aircraft and the ice surface and the distance from the ice surface to the bedrock. From those distances the ice thickness is calculated. When the conditions permit acquisition of laser scanner data of the ice surface, the ice-sounder surface measurements are

replaced by the laser measurements having much higher accuracy. The aircraft position was recorded by three onboard geodetic GPS receivers sampling at 1 Hz corresponding to a flight distance of approximately 70 m. The three GPS receivers were connected, via splitters, to either the front or the rear aircraft GPS antenna.

A fixed GPS station established near Kangerlussuaq airport was used as reference station. The sampling frequency of the laser-scanner was 40 scan lines each with 250 measurements per second while the ice-sounder recorded 3.125 samples/second (after pre-processing).

2.2 Data coverage

The grey lines in Figure 1 show the flight tracks, the green lines indicate the areas where good radar returns were detectable at the bed. A complete coverage of GPS positions was obtained along all flight tracks within the mapped ice margin sector. Laser scanner (lidar) data was acquired on all lines except one in the north-eastern most area where data from the back-up single beam altimeter has been used. Data from Julian day 280 (October 6th) is only delivered as files with the vertical line (nadir to the aircraft) since problems with the INS system caused degradation of the angular accuracy. The ice-sounding radar worked continuously during the complete flight mission, but was not active during the transits between the airport and the ice edge. The radar was not able to detect the bottom in some areas near the ice edge mainly due to heavily crevassed ice.

Radar and lidar both work by emitting electromagnetic pulses and measuring the time delay from pulse transmission to the echo returns. The locations of both instruments are fixed using a GPS system and their attitudes are determined using the INS system. The lidar pulse does not penetrate the ice surface and thus only measures the ice surface elevation. The radar pulse does penetrate the ice yielding two reflections: one from the surface of the ice and one from the subglacial bed. The radar pulse is both scattered and attenuated by liquid water and air in crevasses and voids. This poses a challenge when mapping the subglacial bed, and may explain the poor coverage over parts of the ice sheet (see Figure 3).

2.3 GPS data

The GPS position data was processed by using a PPP (Precise Point Positioning) software developed partly at Wuhan University and partly at National Space Institute, DTU Space, providing latitude, longitude and height above the WGS84 ellipsoid of the GPS antennas. The solutions were compared with differential GPS solutions from Trimble GPSurvey 2.35 to evaluate the robustness of the positions. Both PPP and GPSurvey rely on precise GPS products from IGS (International GNSS Service).

Data from the different GPS receivers was compared and quality controlled, and the best solution selected for further use. The GPS data were transferred to the laser scanner and ice-sounder instruments by adding the positions of these instruments inside the aircraft relative to the GPS antenna positions to the GPS data.

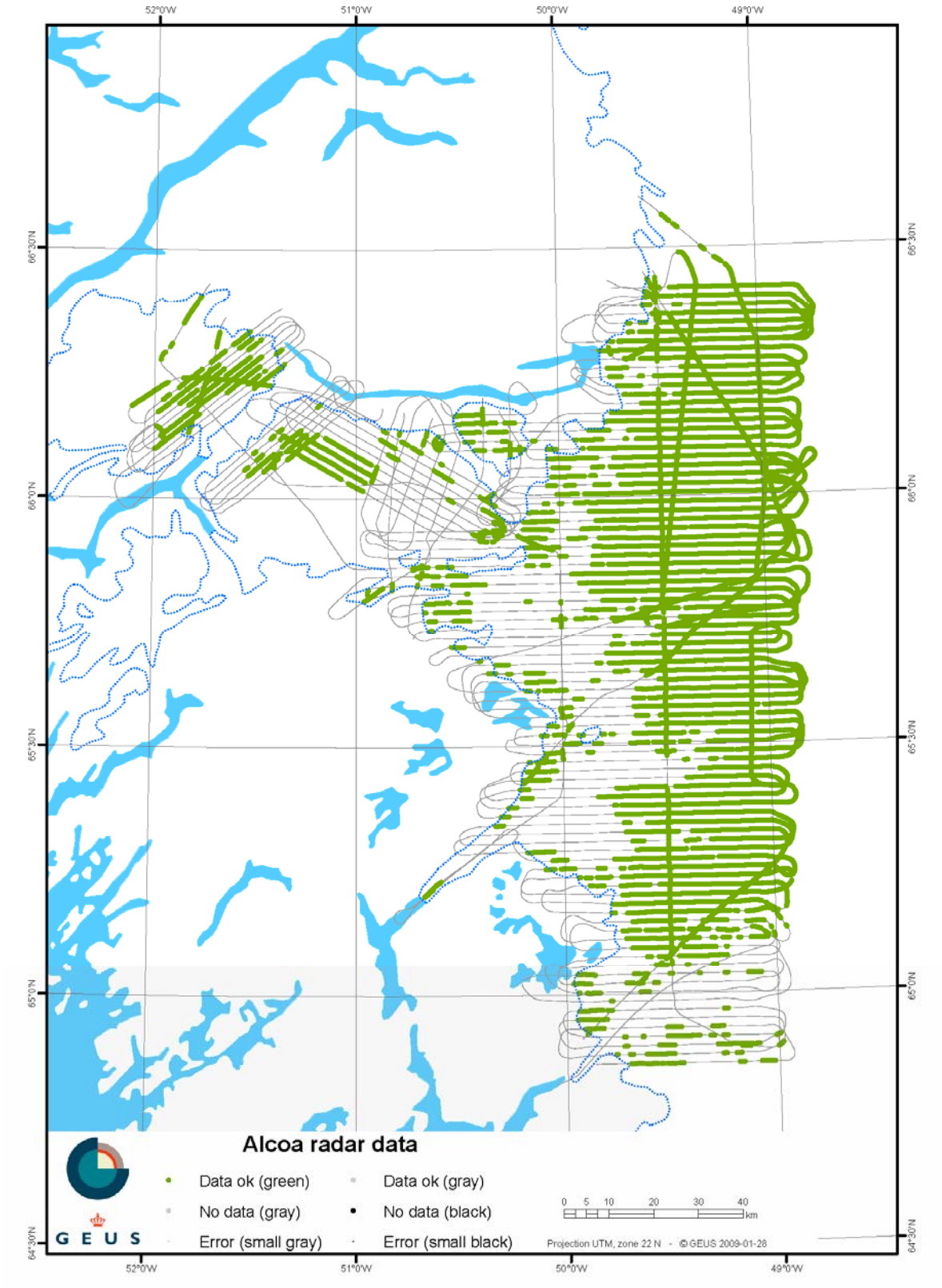

Figure 1. Flight lines from the ice sheet survey in 2008. Green lines show where bed returns were detected, the grey lines indicate the flight tracks. The blue dashed line indicates the ice margin.

2.4 Lidar data

Surface elevation data was derived from laser altimeter measurements made concurrently with the radar measurements and using the same INS and GPS set up to derive positioning information. The Riegl scanning laser used to make the elevation measurements, provides cross-track scans with a range accuracy better than 5 cm. Absolute elevations are given with a precision of ±0.3 m following processing. The laser operates in the near-infrared wavelength band and has a scan angle of 60°, giving a swath width similar to the flight elevation above the ground. Over the glacier surface, a typical value of this distance was 300 m. Roll, pitch, heading, and yaw of the aircraft were recorded at 50 Hz by a Honeywell H764-G, medium-grade INS (Inertial Navigation System). The orientation and the position of the aircraft with respect to the earth fixed reference system are used to exactly map each laser measurement to a position on the surface.

Two files were produced: a file containing a third of the observed values in every third scan, and a file containing one value per three scans representing the vertical distance between the laser scanner and the surface. In a few areas clouds were present in the processed laser scanner data. To remove the clouds data is passed through a filter that fits a flat surface to the laser points and then rejects points at some distance above this surface. If the cloud cover has a flat top the filter will wrongly see this as the true surface and hence accept the data, these data are therefore edited manually.

Data quality control on the lidar data has been preformed by comparing data from crossing tracks. The mean of these crossings varied from −0.13 m to 0.30 m, with the standard deviation varying between 0.05 m and 0.19 m. The larger values resulted from crevassed areas. Similar cross-over tests have been done for each flight internally giving similar or better results.

2.5 Radar data

The ice-sounding radar data acquisition consists of transmitting pulses at a pulse repetition frequency of 10kHz (i.e. the sampling in the flight direction) and sampling the returned echo at 75MHz in range producing 4096 samples per transmitted pulse. While internal scattering masks the desired echo, reflection and absorption within the ice-sheet reduces the strength of the returned echo. Substantial processing is therefore required to produce a radargram that makes detection of the ice-sheet bottom echo possible. This radargram processing is done both on-line during acquisition and off-line using software developed at the Microwave & Remote Sensing division, DTU-Space. An example of a radargram obtained by the ice-sounder is displayed in Figure 2, where the horizontal direction represents the time with a spacing of 320 ms per line (i.e. 22.4 m spacing at aircraft velocity 70 m/s). The vertical direction shows propagation time of the radar pulse with a spacing of 80 ns per line of the radar pulse. This represents vertical distances but not by simple scaling because the speed of light within the ice sheet is lower than in free air. The transmit pulse is also visible in the radargram, because echo data sampling is started before the transmit pulse begins. This early starting of data sampling ensures calibration of the propagation delay.

The processing of the ice-sounder data was performed by using a semi-automatic layer (bottom and surface) detection program developed at the Microwaves & Remote Sensing

division, DTU Space. The detection program detects each layer individually, hence the following detection procedure is performed for both surface and bottom. The detection processes is initiated by the user selecting a pixel in the radargram that is part of the layer to be detected. This pixel is located in one particular vertical line. The automatic part of the programme then selects the pixel (left or right) within a specified search angle in a neighbouring vertical line that shows the strongest contrast to its neighbouring samples in the same line. This second pixel then becomes the basis for the automatic selection of the third pixel and so forth. There may be multiple echoes from the bedrock at some locations with rough bedrock. In such cases it may be impossible to se which echo is from vertical beneath the aircraft and which echo comes from the bedrock slightly off the flight track. This algorithm works well in areas with good layer echoes. In other areas the automatic detection loses track of the layer and the user is then required to manually set the pixel for each vertical line. As the layer (both bottom and surface) may not be detectable everywhere, the outcome of this process is a number of intervals of consecutive vertical lines with a pixel defining the layer. The positions of all these pixels in terms of UTC-time, GPS position, and propagation time are recorded to a file.

The precision of the lidar is an order of magnitude higher than the radar, but can only be used to calculate the surface elevation. The radar elevations are known with a resolution better than 40 m and lidar elevation are given with a precision of ± 0.3 m. In places with very strong reflections, e.g. bare rock, the radar resolution may approach 5-10 m.

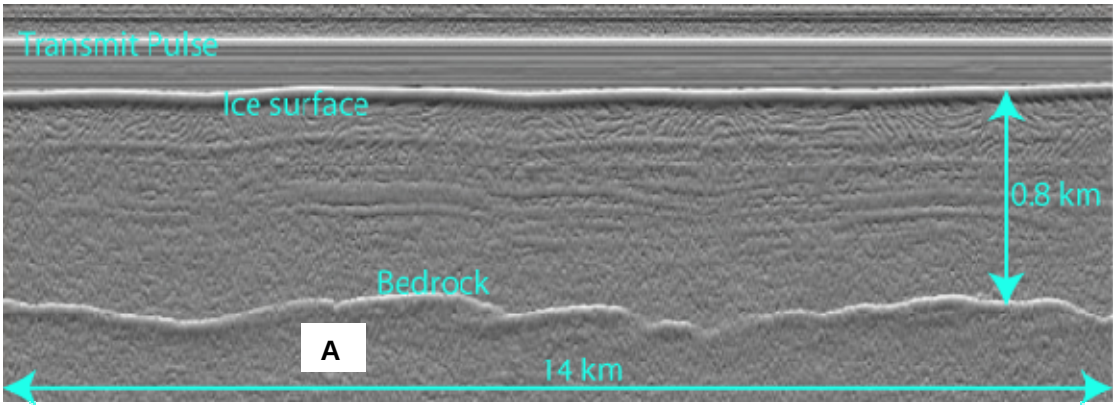

Figure 2. *Radargram illustrating bed and surface topographic traces as well as the transmit pulse.*

2.6 Deriving ice surface, ice thickness and bottom elevation

UTC-time (from GPS time) is recorded by all of the GPS-position-, laser scanner-, and, ice-sounder instruments and is used as reference for aligning the three different types of observations. At the time of the ALCOA flight mission, the GPS-time is given as UTC-time plus 14 seconds.

The calculation of ice thickness and bedrock elevation requires the surface elevation to be known; hence ice thickness and bedrock elevation is not calculated in areas where the ice surface could not be measured with neither the scanner nor the radar.

The ice surface elevation can be measured with either the scanner or with the radar, but the two sensors do not detect the same surface. The scanner detects the optical surface usually perceived as the surface while the radar pulse is reflected approximately 12 m below the optical surface. This difference has been measured by comparing measurement over the Kangerlussuaq runway with measurements over the ice. As the scanner is far more accurate than the radar, scanner data has been used for calculating the surface elevation where available. However, due to fog or high aircraft altitude scanner data was not available everywhere and radar data was then used instead. As the 12 m difference only applies over ice and as all radar data recordings including parts without ice were requested, no surface elevation correction was applied in areas where radar data was used. Instead the radar data product contains information as to which sensor was used for each calculation of the surface elevation. However, this surface difference was corrected for in the calculation of ice thickness and bottom elevation as shown below.

The ice surface elevation (given as height above the ellipsoid) of a point along the flight track is calculated by subtracting the aircraft to surface distance d_{surf} measured by the laser scanner from the GPS-measured aircraft ellipsoidal height. The horizontal position of the surface point is given by the horizontal GPS coordinates.

The ice thickness of a point along the flight track is given by

$$d_{ice} = 84.5\ (T_{bot} - T_{sur}) + 12$$

where d_{ice} is the thickness of the ice in meters. T_{bot} is the propagation time (echo delay) in microseconds of the radar signal bottom echo and T_{sur} is the propagation time in microseconds of the radar signal surface echo. T_{bot} is measured by the radar.

When laser data are available T_{sur} is calculated by

$$T_{sur} = T_{pulse} + (d_{surf} + d_{cable} + 12) / 150$$

where T_{pulse} is the propagation time in microseconds of the radar transmit pulse, d_{surf} is the distance in meters from scanner to ice surface and d_{cable} is the equivalent free air length of the radar to antenna cable.

When laser data are not available, T_{sur} is taken from the radar measurements and is calculated as

$$d_{surf} = 150\ (T_{sur} - T_{pulse}) - d_{cable} - 12$$

in order to provide the surface elevation. The bottom elevation is obtained by subtracting the ice thickness from the surface elevation. All elevations are in WGS84 ellipsoid coordinates.

2.7 Ice margin definition

The elevation models and maps presented in this report (Figures 1, 6, 7, 8, 9 and 10) include, for reference purposes, a digitised line indicating the ice margin. This is derived from GEUS topographic maps of Greenland, which were constructed from aerial photographs taken in the late 1980's. The comparison in Figure 3 indicates the ice extent has changed little since then. The ice margin was not delineated specifically in this work, as this was not a part of the scope, but could be obtained from recent high-resolution satellite imagery.

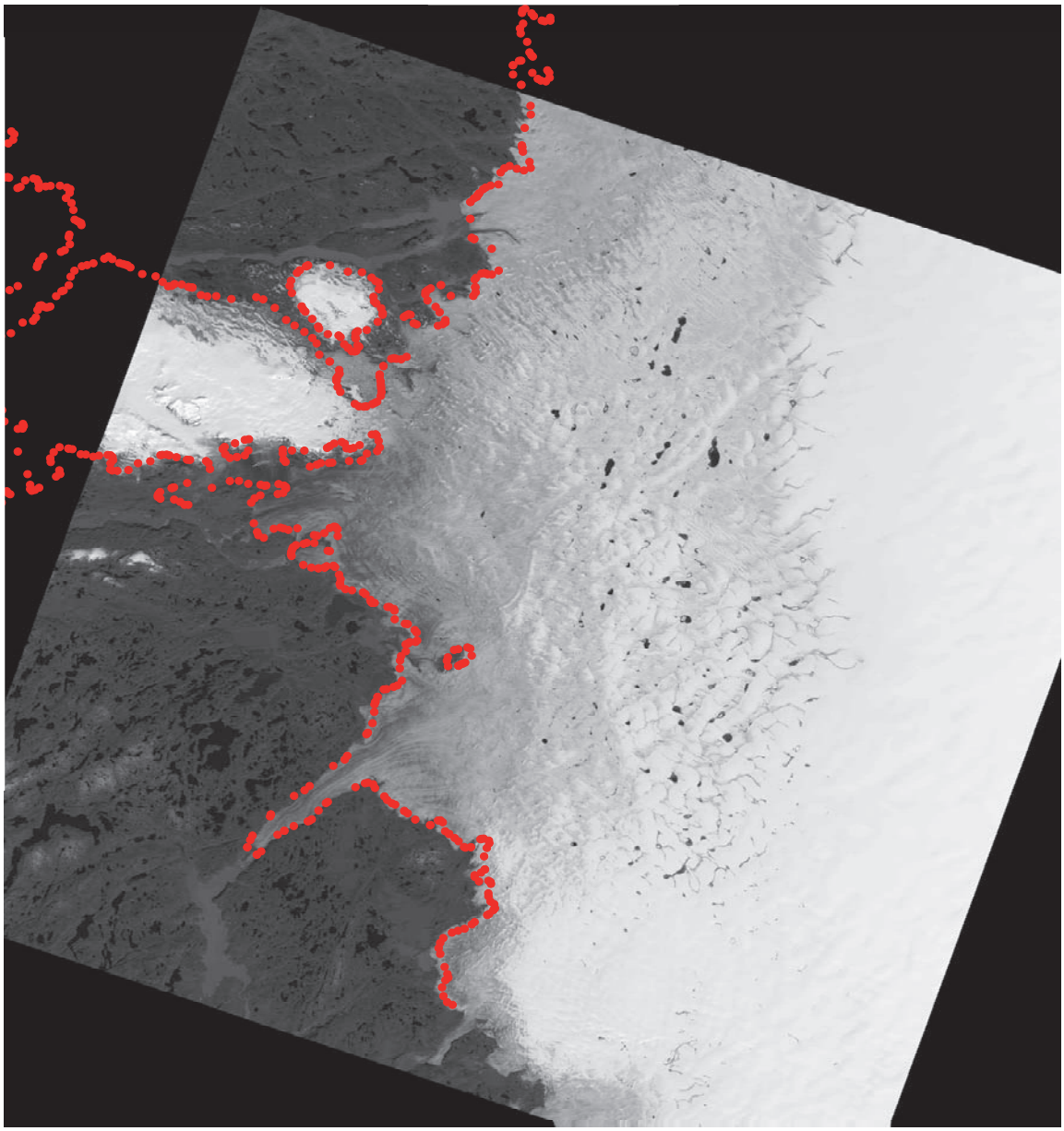

Figure 3. *Satellite image taken on the 3rd August 2001, retrieved from the USGS Landsat archive 10th February, 2009. The image is presented in grayscale to enhance the contrast between areas of snow, firn and old glacier ice. The dotted red line is the ice margin as it was derived from aerial photograph from 1985, signifying that little change has occurred in the area. The dark spots on the ice sheet are surface lakes, note that many of them are linked to surface drainage routes. The presence of so much surface water may explain some of the poor radar returns.*

3. Digital elevation modelling

Previous work (Mottram and others, 2008; Ahlstrøm and others, 2005) with similar data sets from Greenland has shown that the geostatistical interpolation method known as block kriging is superior for creating regular grids from the airborne radar and lidar data. Kriging is used to estimate elevation at an unobserved location from observations at nearby locations. In making each calculation, the algorithm applies more weight to the values of locations closer to the unknown point and less weight to observations from farther away. It is a particularly powerful technique for topographic interpolation, as the algorithms can also be used to take into account the directional variability of topography. That is, in some directions topography may have greater variability than in other directions around a known point, this is particularly true in areas of high relief. Although the principle is simple, there are some extra complexities, particularly when using data for which there is substantial uncertainty, as with the absolute basal elevations.

The core of the kriging technique is the semivariogram, usually abbreviated to the variogram. The variogram is a function of how quickly elevation changes on average in any given direction. Variograms actually represent three variables; two independent variables, the direction and the separation distance; and one dependent variable known as the variogram value, a function of the two independent variables. The plotted variogram is a radial slice (like a piece of pie) from a grid of these 3 variables and it is therefore necessary to examine multiple variograms when fitting a model as it is difficult to both draw a three-dimensional surface and to fit a three dimensional function to it. By taking slices, an XY plot can be used to work with the directional experimental variogram. Ultimately the variogram model must be applicable to all directions fitting the model. In the sections below, some of the variograms for the surface and basal datasets are examined more closely. In these the lag distance (the separation distance between pairs of points) is plotted on the x-axis, and the variogram function is shown on the y-axis. The plot therefore shows how elevations vary with distance from a given point. The blue lines indicate the model fit and the black lines show how the data fit.

3.1 Characterization of the basal topography

The DEM of the subglacial topography is based on a kriging model using a rational quadratic function (Kitanidis, 1997), with a small nugget effect to account for the imprecision of the radar data returns (better than 40 m resolution). A report generated automatically by the software during the kriging process is given in Appendix A, showing the important statistics calculated for the dataset based on the variogram model.

The variogram model was initially developed using basal data from below the main ice sheet and then compared with a second kriging model developed for the smaller ice caps external to the main ice. The very sparse data availability in the Sukkertoppen region made it difficult to compare exactly, but both do contain similar elements. This would be expected as the landscape in these areas does show some self similarity (also compare with other previously glaciated terrain such as the Canadian shield). The algorithm was then applied to the full basal dataset and the output gridded at a 2 km resolution.

The semivariograms plotted for four different directions are shown in Figure 4, each graph also shows how the model fits to the dataset (the blue line).

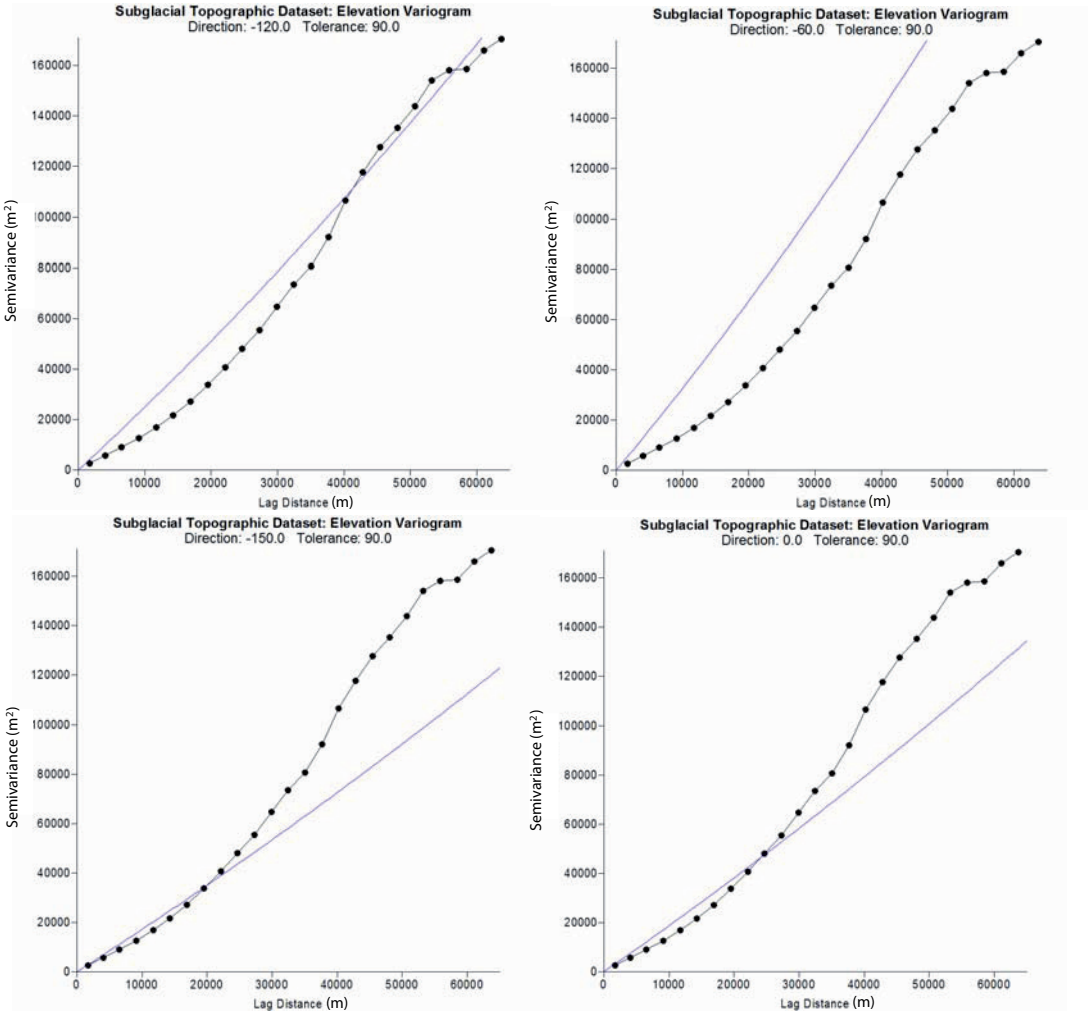

Figure 4. *Four variograms illustrating the fit of the model curve (blue line) to the plotted data points ín four different directions for the bedrock topography.*

3.2 Characterization of the surface topography

To generate the surface model an ordinary linear kriging model gave by far the best interpolation result of any kriging model. It is also the same one used in an earlier project related to hydropower in the Paakitsoq area (Mottram *et al.*, 2009) of the Greenland ice sheet. The generally good fit of the linear model is probably largely due to the way ice flow acts to linearise and smooth out topographic variability, as shown in the variograms in Figure 5.

The surface dataset consisted of almost 397,000 individual data points. This made it impractical to work with, so for the purposes of plotting up the variograms and determining the correct model to use, the dataset was once again divided into three parts. All three parts gave very similar resultant variograms.

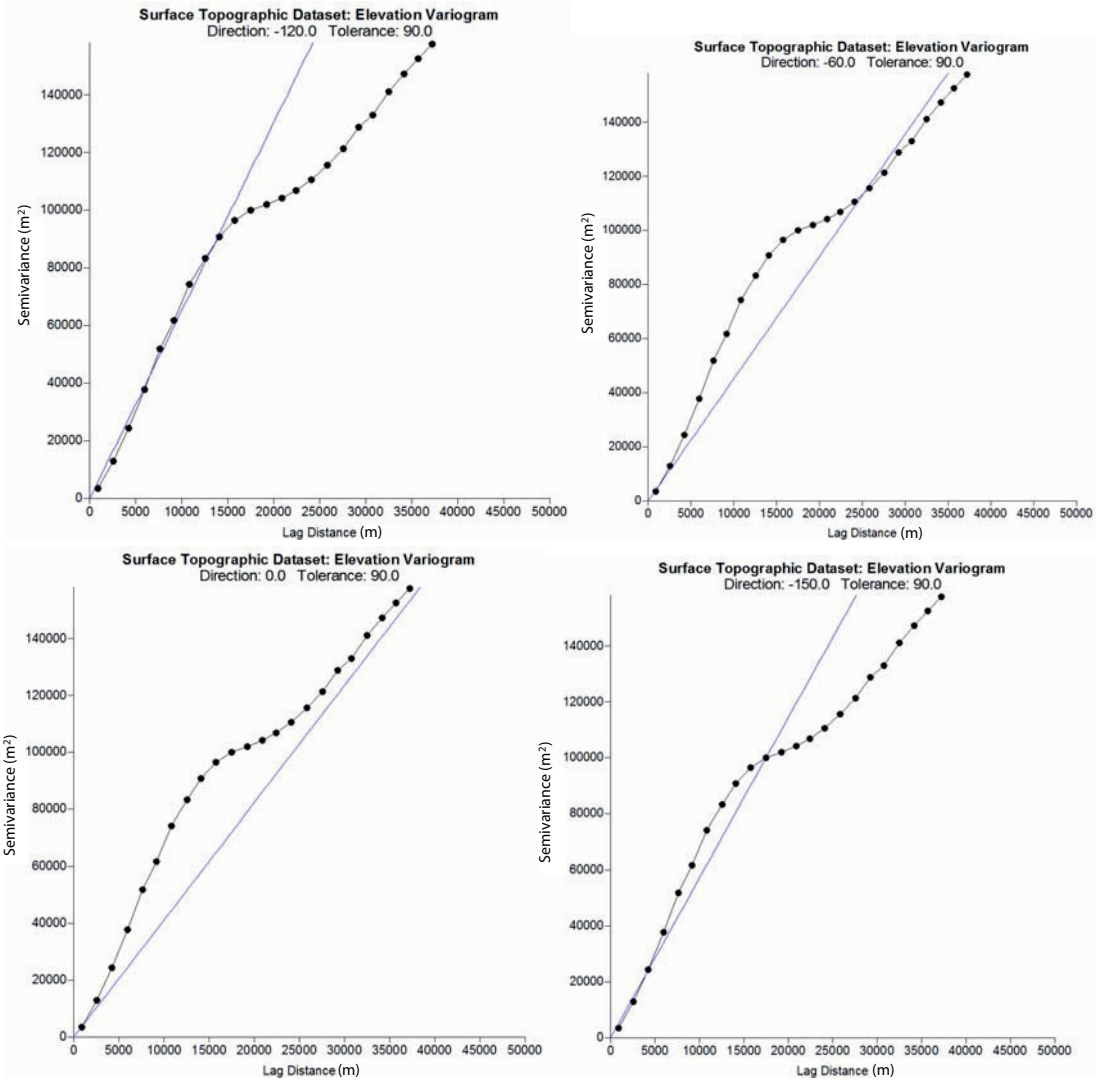

Figure 5. *Linear variogram models for the ice surface topography.*

4. Results

4.1 Surface topography DEM

The DEM for the surface topography is presented in Figure 6 below. The map is created from the gridded interpolated dataset produced by applying the kriging algorithm over the dataset. Further information on the grid properties are given in Appendix D.

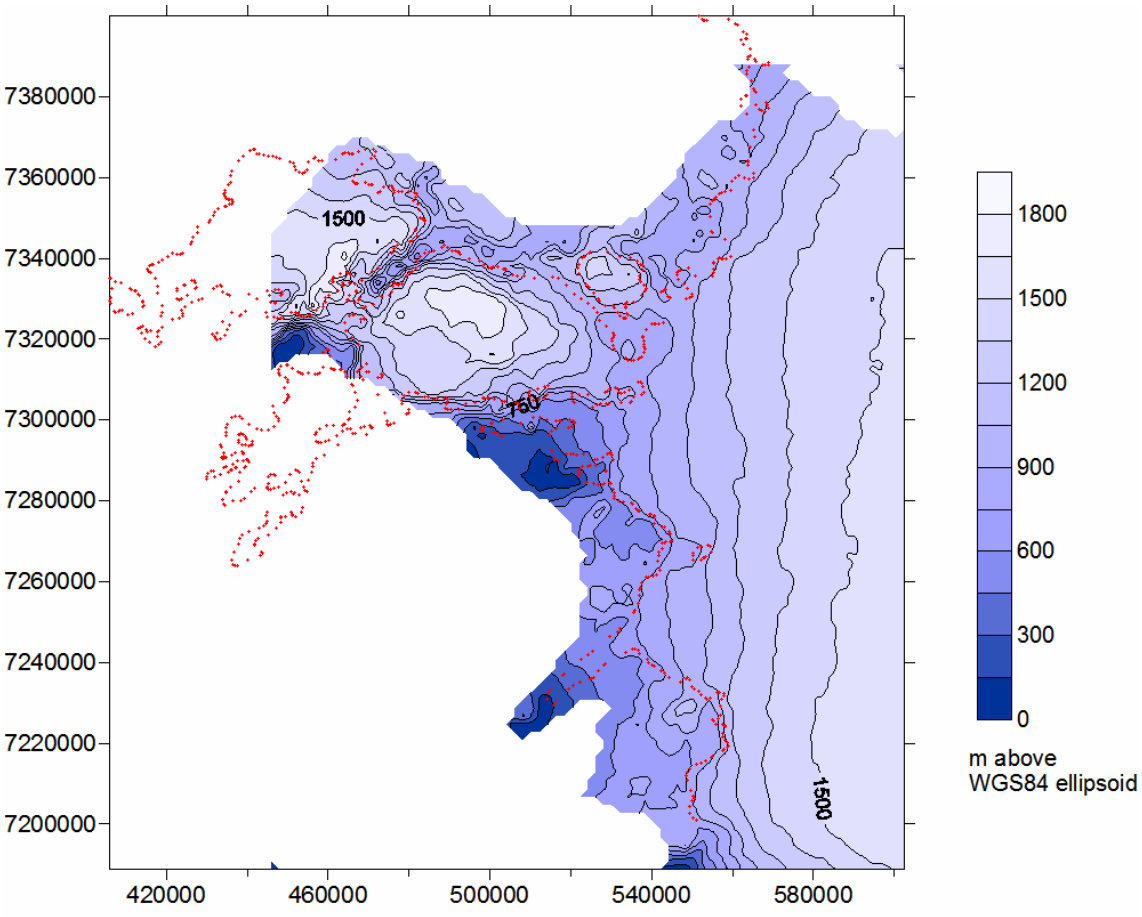

Figure 6. *Map of the ice surface topography showing contours in intervals of 150 metres above the WGS84 ellipsoid. The coordinates are in UTM Zone 24 projection. The red dotted line indicates the ice margin (see Section 2.2) The grid was blanked after plotting to exclude areas for which there was no data.*

The shape of the contours largely echo those presented on topographic maps of the region and are in fact very much in line with what would be expected in this area, with the gently sloping ice sheet margin. In spite of smoothing the mapped contours, they are somewhat irregularly shaped in places. This is probably due to the surface lakes, which form in and enlarge local depressions thus causing the surface to be less smooth in the firn zone. Other irregularities may be caused by underlying basal topography or may be artefacts from the data collection and processing work.

The data coverage is very good in the surface dataset (see Figure 7), improving the confidence in the resulting DEM.

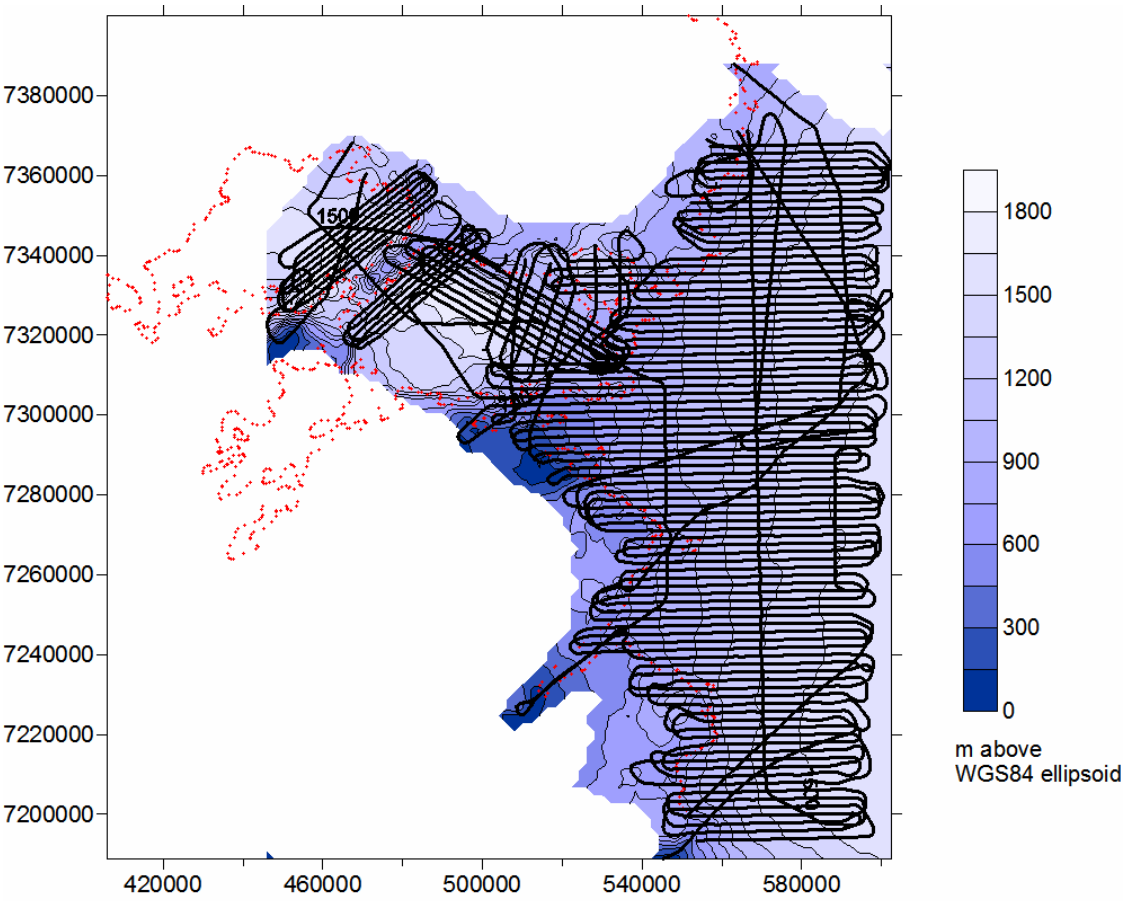

Figure 7. *Map of the ice surface topography showing contours in metres above WGS84 ellipsoid .The coordinates are in UTM Zone 24 projection. The red dotted line indicates the ice margin, the black lines indicate the flight lines forming the basis of the data coverage used to construct this map. Lidar data from the turns were excluded.*

4.2 Basal topography DEM

Figure 8 presents the map of subglacial topography, defined from the radar dataset. The map is created from the gridded interpolated dataset produced by applying the kriging algorithm over the dataset. Further information on the grid properties are given in Appendix C. Although the dataset had less total coverage, there were still some 299,000 data points which were used to construct the gridded dataset.

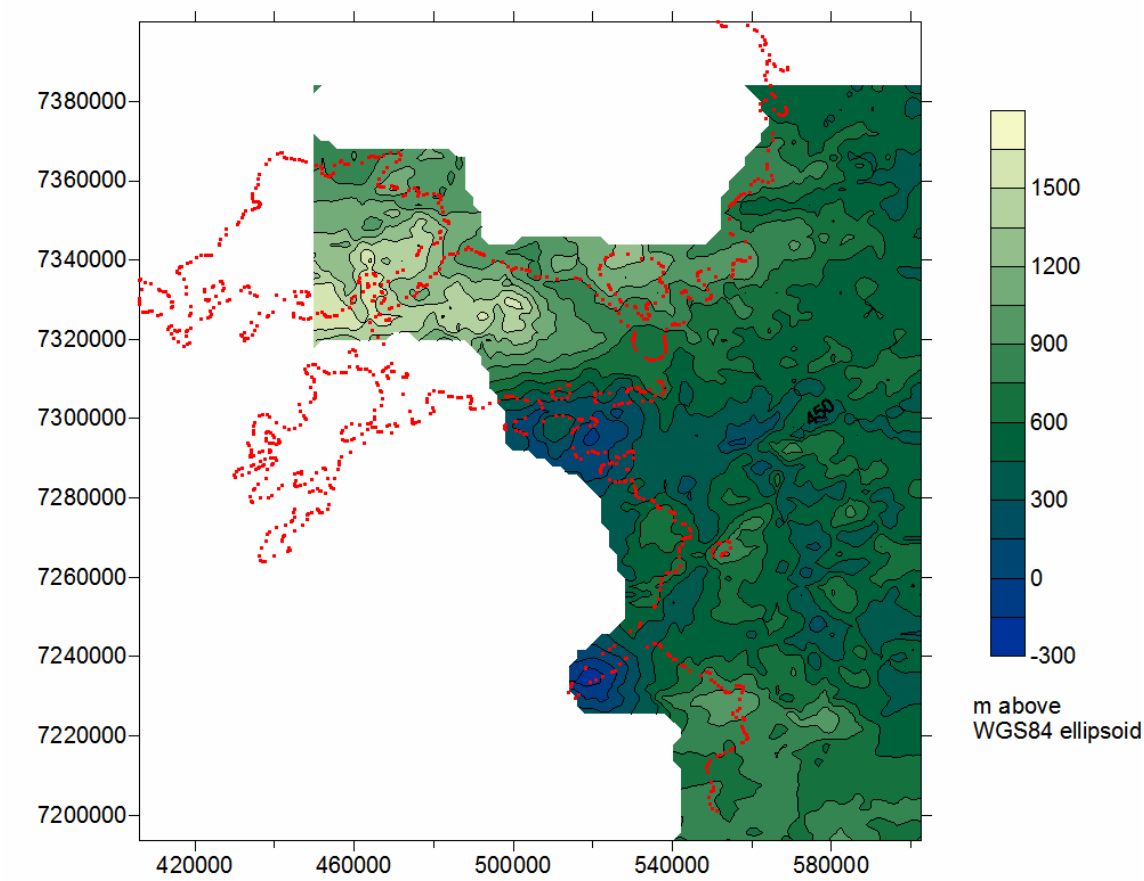

Figure 8. *Map of subglacial topography showing contours in intervals of 150 metres above WGS84 ellipsoid. The coordinates are in UTM Zone 24 projection. The red dotted line indicates the ice margin (see Section 2.2). The grid was blanked after plotting to exclude areas for which there was no data.*

The basal topographic map is based on a more sparse data coverage (see Figure 9), but some of the visible features are consistent with surface features, for instance the raised ground around the nunatak in the ice sheet margin, and the higher ground beneath Sukkertoppen and the other small ice cap. These features would not exist under current climate without higher elevations being present. Similarly, the deep trench to the south extending along an axis from south west to north east, is a typical feature of the Greenland ice sheet and indicates that important dynamic changes may be mediated along this topographic low. The somewhat complex topography consisting of small individual hillocks is reminiscent of 'kame and kettle' topography, often found in formerly glaciated regions where glacial scouring and consequent deposition of sediment leave an uneven hummocky topography behind. As similar features are seen in other locations in Greenland (Ahlstrøm *et al*., 2007; Mottram *et al*., 2009), and the data coverage sufficiently complete in these areas, we conclude the smaller scale features are likely to reflect real subglacial topography.

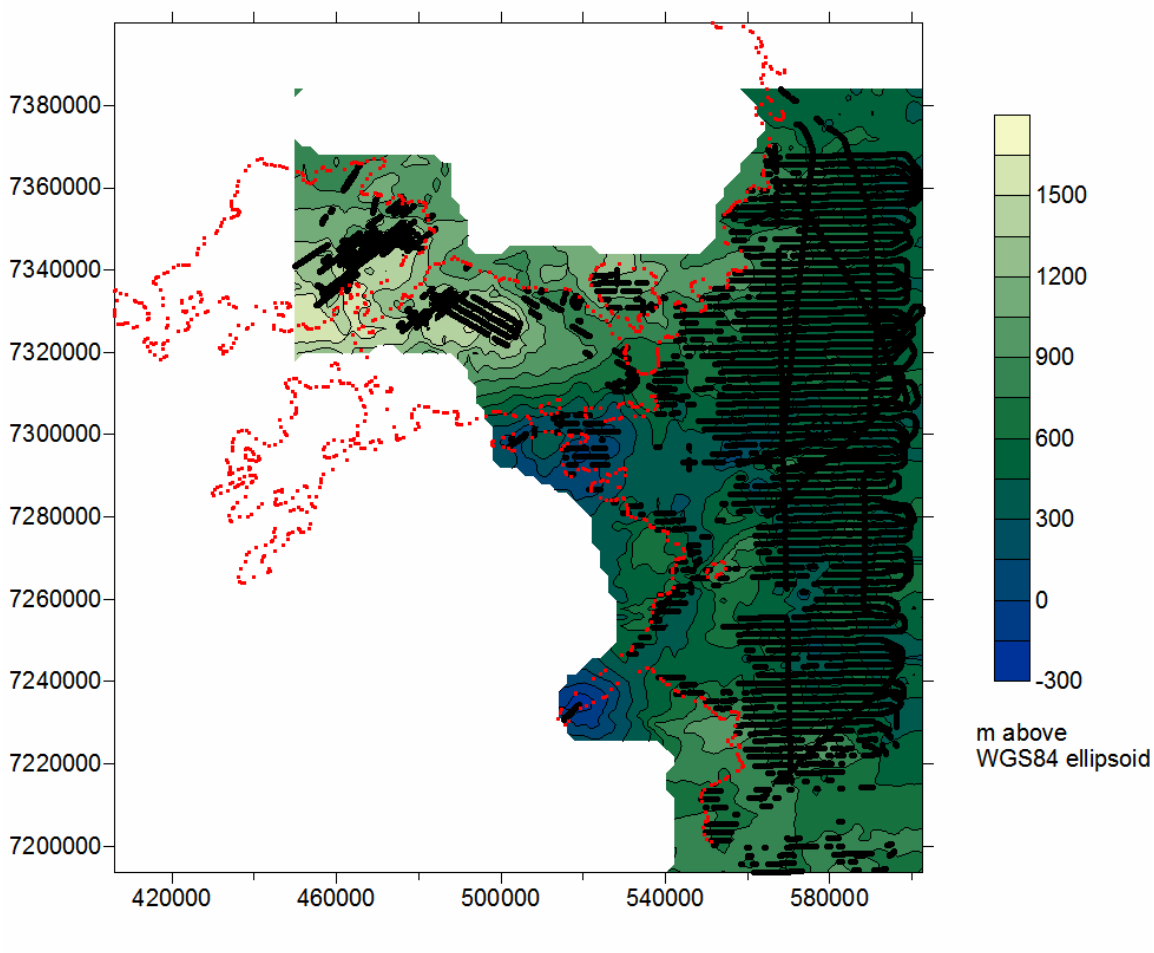

Figure 9. *Map of the subglacial topography showing contours in metres above WGS84 ellipsoid. The coordinates are in UTM Zone 24 projection. The red dotted line indicates the ice margin, the black lines indicate the data coverage used to construct this map.*

4.3 Ice thickness model

The map of ice thickness presented in Figure 10, was created by subtracting the basal elevation grid from the surface elevation grid, rather than by direct measurement. It thus reflects the variability shown by both datasets.

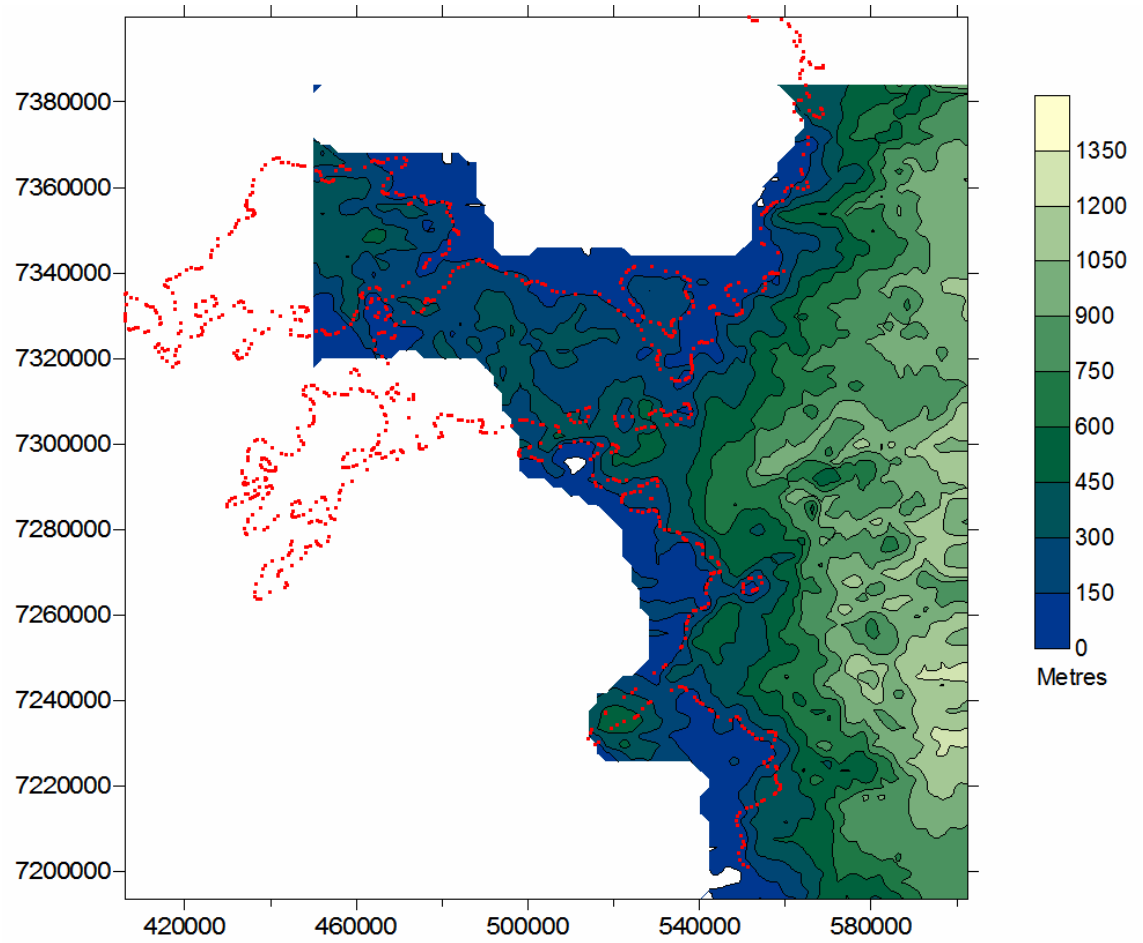

Figure 10. *Map of the ice thickness derived from the subglacial and ice surface elevations. Contours indicate ice thickness in metres. The coordinates are in UTM Zone 24 projection. The red dotted line indicates the ice margin (see Section 2.2). The grid was blanked after plotting to exclude areas for which there was no data.*

5. Summary

The surface and subglacial topography of this area of the Greenland Ice Sheet are presented in this report along with details about the collection and analysis of data and the post-processing and interpolation methods used to build substantial DEMs of the area. The actual data was delivered on the 27th February, 2009. This report is therefore a complimentary summary giving further details of the analysis which may be of use when interpreting and using the data.

6. References

Ahlstrøm, A.P., Bøggild, C.E., Mohr, J.J., Reeh, N., Christensen, E.L., Olesen, O.B., Keller, K. (2002). Mapping of a hydrological ice sheet drainage basin on the West Greenland ice-sheet margin from ERS-1/-2 SAR interferometry, ice radar measurement and modelling. Annals of Glaciology 34(309-314).

Ahlstrøm, A.P., J.J. Mohr, N. Reeh, E.L. Christensen, R.LeB. Hooke (2005): 'Controls on the basal water pressure in subglacial channels near the margin of the Greenland ice sheet', Journal of Glaciology, 51(174), 443–450.

Kitanidis, P. K. (1997). Introduction to Geostatistics. Cambridge, Cambridge University Press.

Mottram, R., Nielsen, C., Ahlstrøm, A.P., Reeh, N., Kristensen, S.S., Christensen, E.L., Forsberg, R and L. Stenseng (2009). A new regional high-resolution map of basal and surface topography for the Greenland ice sheet margin at Paakitsoq, West Greenland Annals of Glaciology, 50, 51 (in press)

Reeh, N., Ahlstrøm, A. (2005). Nordic Project on Climate and Energy, Subproject Hydro-power, Snow and Ice. Danish National Space Centre, Technical University of Denmark.

Appendix A: Basal Dataset Variogram Grid Report

Variogram Grid

Maximum Lag Distance:	65000
Angular Divisions:	180
Radial Divisions:	100

Data Counts

Active Data:	49728
Original Data:	49728

Univariate Statistics

	X	Y	Z
Minimum:	7193516.4	515713.89	0
25%-tile:	7319620.92	565727.17	532.979
Median:	7329617.01	574066.49	740.176
75%-tile:	7339780.18	588150.15	898.305
Maximum:	7369796.58	602497.81	1100.013
Midrange:	7281656.49	559105.85	550.0065
Range:	176280.18	86783.92	1100.013
Interquartile Range:	20159.26	22422.98	365.326
Median Abs. Deviation:	10113.76	11477.88	173.461
Mean:	7320442.856194	574372.09094252	689.46775852638
Trim Mean (10%):	7325340.4291071	575432.20268791	700.06688017249
Standard Deviation:	37797.943336583	17085.375816768	255.14318030326
Variance:	1428684520.4755	291910066.8002	65098.042455263
Coef. of Variation:			0.37005817479934
Coef. of Skewness:			-0.62598343851105

Inter-Variable Correlation

	X	Y	Z
X:	1.000	0.108	0.109
Y:		1.000	0.847
Z:			1.000

Inter-Variable Covariance

	X	Y	Z
X:	1428684520.4755	69470278.580276	1052090.3958761
Y:		291910066.8002	3694284.5922498
Z:			65098.042455263

Planar Regression: Z = AX+BY+C

Fitted Parameters

	A	B	C
Parameter Value:	0.000122441030417260	.012626418160002	-7459.1170076384
Standard Deviation:	1.6153916389621E-005		3.573727749027E-005
	117.82799524766		

Inter-Parameter Correlations

	A	B	C
A:	1.000	0.108	-0.985
B:		1.000	0.066
C:			1.000

ANOVA Table

Source	df	Sum of Squares	Mean Square	F
Regression:	2	2325997415.4086	1162998707.7043	63466
Residual:	49725	911198039.80714	18324.746904116	
Total:	49727	3237195455.2158		

Coefficient of Multiple Determination (R^2): 0.71852239000922

Nearest Neighbor Statistics

	Separation	|Delta Z|
Minimum:	2.00449494827	0
25%-tile:	22.662259375483	0.15200000000004
Median:	23.990133388532	6.465
75%-tile:	25.290577297178	6.957
Maximum:	50.590283652175	148.273
Midrange:	26.297389300223	74.1365
Range:	48.585788703905	148.273
Interquartile Range:	2.6283179216946	6.805
Median Abs. Deviation:	1.3106907086455	6.2479999999999
Mean:	23.822900775274	5.0350710263835
Trim Mean (10%):	23.930483366409	4.7652808785414
Standard Deviation:	1.9043885025056	5.278845010139
Variance:	3.6266955684755	27.866204641069
Coef. of Variation:	0.079939404544813	1.0484152025817
Coef. of Skewness:	-1.3792039515629	1.7031824141213
Root Mean Square:	23.898897399609	7.295076756402
Mean Square:	571.15729691705	53.218144881796

Complete Spatial Randomness

Lambda:	3.2505604304133E-006
Clark and Evans:	0.085902095801961
Skellam:	580.0892736061

Appendix B: Surface Dataset Variogram Grid Report

Variogram Grid

Maximum Lag Distance:	38000
Angular Divisions:	180
Radial Divisions:	100

Data Counts

Active Data:	59254
Original Data:	59254
Excluded Data:	0
Deleted Duplicates:	0
Retained Duplicates:	0
Artificial Data:	0

Univariate Statistics

	X	Y	Z
Minimum:	446084.01840567	7293084.3527849	29.008
25%-tile:	470024.05588814	7323307.5455839	1012.275
Median:	487230.89891228	7333853.6092618	1283.796
75%-tile:	508075.45109255	7342636.608807	1537.821
Maximum:	536774.27461519	7362393.1477398	1972.466
Midrange:	491429.14651043	7327738.7502623	1000.737
Range:	90690.256209518	69308.79495484	1943.458
Interquartile Range:	38051.395204417	19329.06322308	525.546
Median Abs. Deviation:	18708.761098389	9503.7068546098	259.67
Mean:	488945.75274007	7332661.4831754	1241.8111451716
Trim Mean (10%):	488712.39438838	7333057.5331931	1261.4639064691
Standard Deviation:	23043.705848631	13955.291638711	356.15015221217
Variance:	531012379.23824	194750164.72147	126842.93092075
Coef. of Variation:			0.28679896584673
Coef. of Skewness:			-0.75032761193261

Inter-Variable Correlation

	X	Y	Z
X:	1.000	-0.441	-0.448
Y:		1.000	0.306
Z:			1.000

Inter-Variable Covariance

	X	Y	Z
X:	531012379.23824	-141913825.4685	-3680820.2325412
Y:		194750164.72147	1521273.0988035

Z:	126842.93092075

Planar Regression: Z = AX+BY+C

Fitted Parameters

	A	B	C
Parameter Value:	-0.0060156035482124	0.0034278575114301	-20952.203793444
Standard Deviation:	6.2663391191207E-005		
	0.00010347306145002	772.74427150065	

Inter-Parameter Correlations

	A	B	C
A:	1.000	-0.441	-0.473
B:		1.000	0.999
C:			1.000

ANOVA Table

Source	df	Sum of Squares	Mean Square	F
Regression:	2	1621015405.7877	810507702.89384	8146.6
Residual:	59251	5894935622.9921	99490.905182901	
Total:	59253	7515951028.7797		

Coefficient of Multiple Determination (R^2): 0.21567668543616

Nearest Neighbor Statistics

	Separation	|Delta Z|
Minimum:	0	0
25%-tile:	22.165317260715	0.28400000000011
Median:	23.616877924078	0.69600000000003
75%-tile:	25.140486712817	1.6310000000001
Maximum:	116.99019015292	262.963
Midrange:	58.495095076461	131.4815
Range:	116.99019015292	262.963
Interquartile Range:	2.9751694521024	1.347
Median Abs. Deviation:	1.488083993746	0.51499999999999
Mean:	23.484525808758	2.163175414318
Trim Mean (10%):	23.58858309413	1.3429745359085
Standard Deviation:	2.5953543804915	5.1517334606082
Variance:	6.7358643603366	26.54035764915
Coef. of Variation:	0.11051338237043	2.3815606568515
Coef. of Skewness:	-0.55669463242918	9.92757041277
Root Mean Square:	23.627501281824	5.5874578765535
Mean Square:	558.25881682259	31.21968552226

Complete Spatial Randomness

Lambda:	9.4268955759638E-006
Clark and Evans:	0.14421025318068
Skellam:	1959.3040158682

Appendix C: Basal Topographic Grid Details

Grid Information

Grid Size:	96 rows x 77 columns
Total Nodes:	7392
Filled Nodes:	4498
Blanked Nodes:	2894

Grid Geometry

X Minimum:	450029.014
X Maximum:	602497.8101
X Spacing:	2006.1683697368
Y Minimum:	7193516.4
Y Maximum:	7383891.09
Y Spacing:	2003.9441052632

Grid Statistics

Z Minimum:	-231.46998126642
Z 25%-tile:	476.57681981097
Z Median:	619.43236039892
Z 75%-tile:	832.89940050603
Z Maximum:	1684.3050374261
Z Midrange:	726.41752807983
Z Range:	1915.7750186925
Z Interquartile Range:	356.32258069506
Z Median Abs. Deviation:	168.36270667216
Z Mean:	674.48059803097
Z Trim Mean (10%):	663.50832263804
Z Standard Deviation:	304.7290832079
Z Variance:	92859.814152728
Z Coef. of Variation:	0.45179814526542
Z Coef. of Skewness:	0.67353237257607
Z Root Mean Square:	740.12424043058
Z Mean Square:	547783.89127294

Appendix D: Surface Topographic Grid Details

Grid Information

Grid Size:	101 rows x 79 columns
Total Nodes:	7979
Filled Nodes:	5022
Blanked Nodes:	2957

Grid Geometry

X Minimum:	446084.0184
X Maximum:	602497.8101
X Spacing:	2005.3050217949
Y Minimum:	7188812.91
Y Maximum:	7387879.96
Y Spacing:	1990.6705

Grid Statistics

Z Minimum:	36.666236817784
Z 25%-tile:	874.08779044981
Z Median:	1192.1322988289
Z 75%-tile:	1432.706242777
Z Maximum:	1862.5211652592
Z Midrange:	949.59370103851
Z Range:	1825.8549284415
Z Interquartile Range:	558.61845232714
Z Median Abs. Deviation:	271.58122228426
Z Mean:	1119.6640122483
Z Trim Mean (10%):	1143.1663878622
Z Standard Deviation:	381.70559471623
Z Variance:	145699.16103767
Z Coef. of Variation:	0.34091083623359
Z Coef. of Skewness:	-0.76277446347848
Z Root Mean Square:	1182.9398384371
Z Mean Square:	1399346.6613616

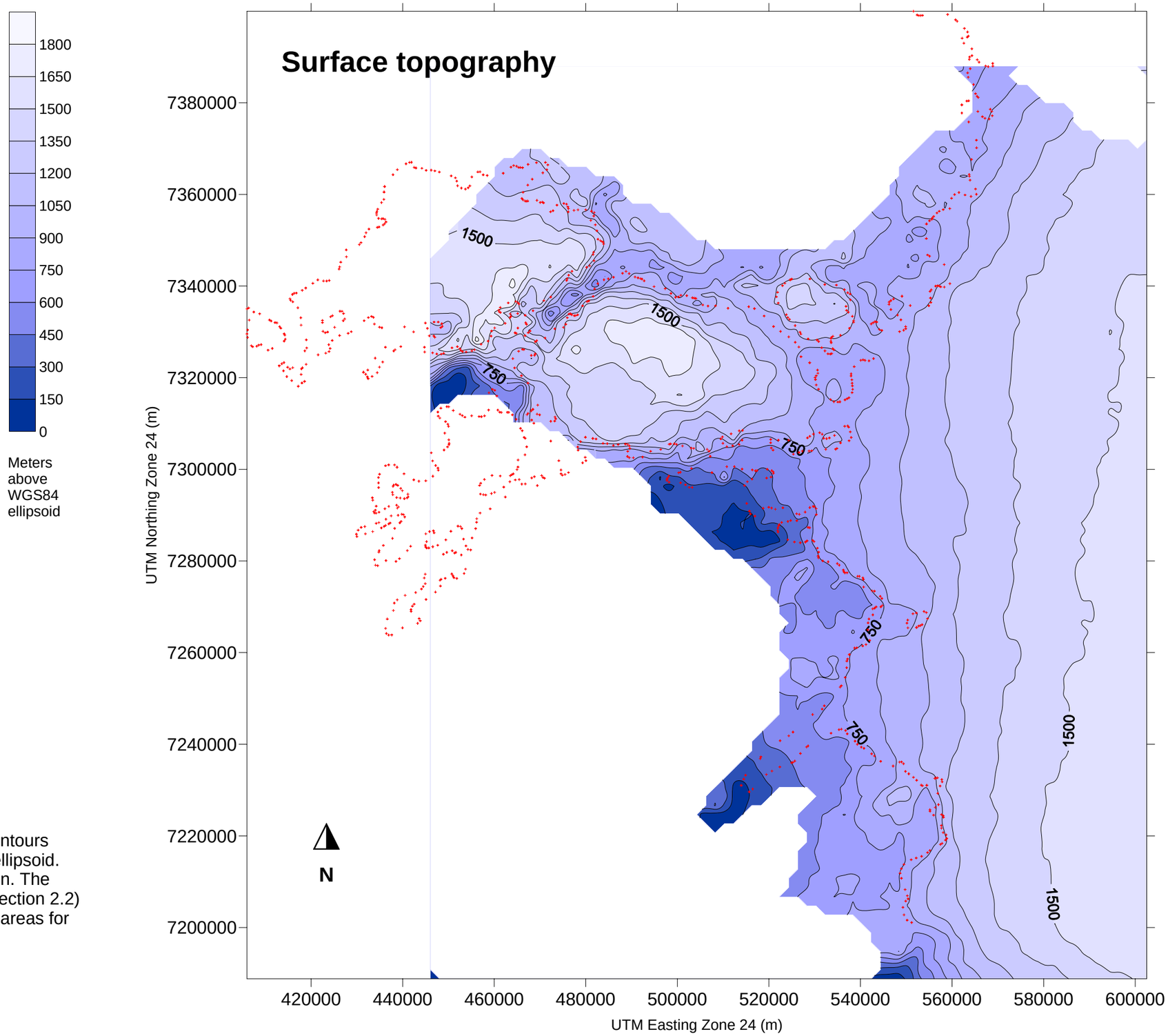

Figure 6 (Enlarged)

Map of the ice surface topography showing contours in intervals of 150 metres above the WGS84 ellipsoid. The coordinates are in UTM Zone 24 projection. The red dotted line indicates the ice margin (see Section 2.2) The grid was blanked after plotting to exclude areas for which there was no data.

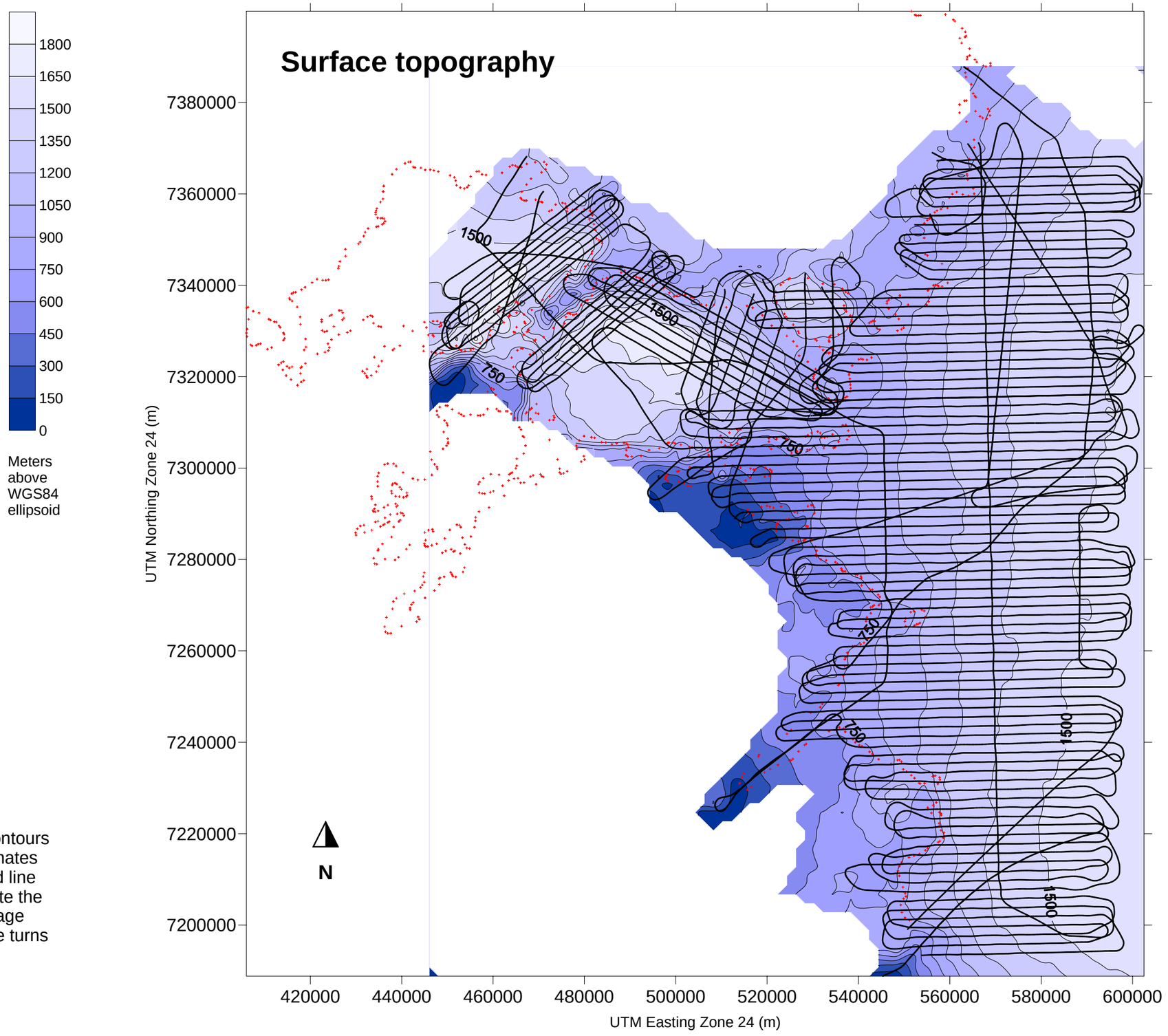

Figure 7 (Enlarged)

Map of the ice surface topography showing contours in metres above WGS84 ellipsoid .The coordinates are in UTM Zone 24 projection. The red dotted line indicates the ice margin, the black lines indicate the flight lines forming the basis of the data coverage used to construct this map. Lidar data from the turns were excluded.

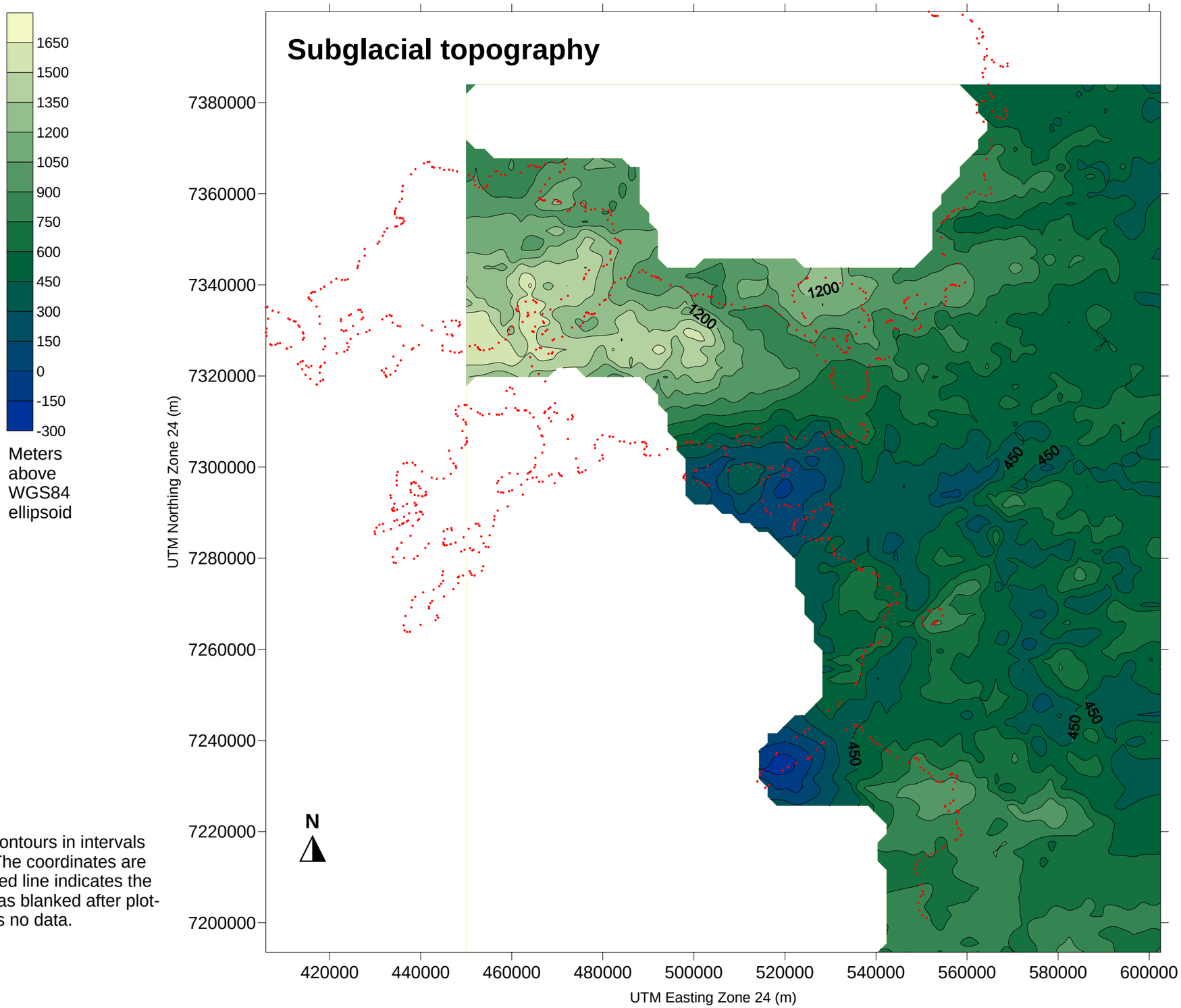

Figure 8 (enlarged version)

Map of subglacial topography showing contours in intervals of 150 metres above WGS84 ellipsoid. The coordinates are in UTM Zone 24 projection. The red dotted line indicates the ice margin (see Section 2.2). The grid was blanked after plotting to exclude areas for which there was no data.

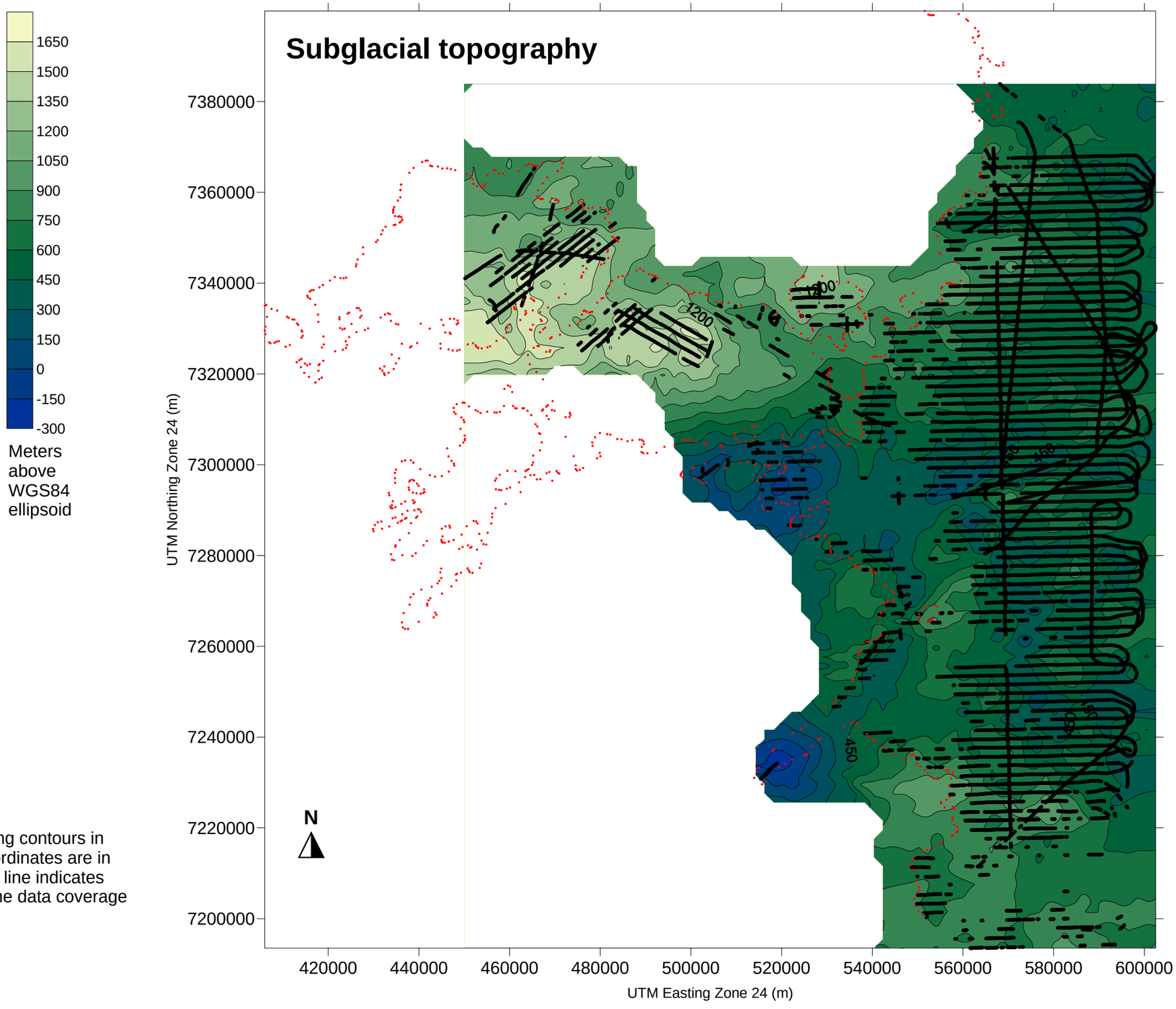

Figure 9 (enlarged version)

Map of the subglacial topography showing contours in metres above WGS84 ellipsoid. The coordinates are in UTM Zone 24 projection. The red dotted line indicates the ice margin, the black lines indicate the data coverage used to construct this map.

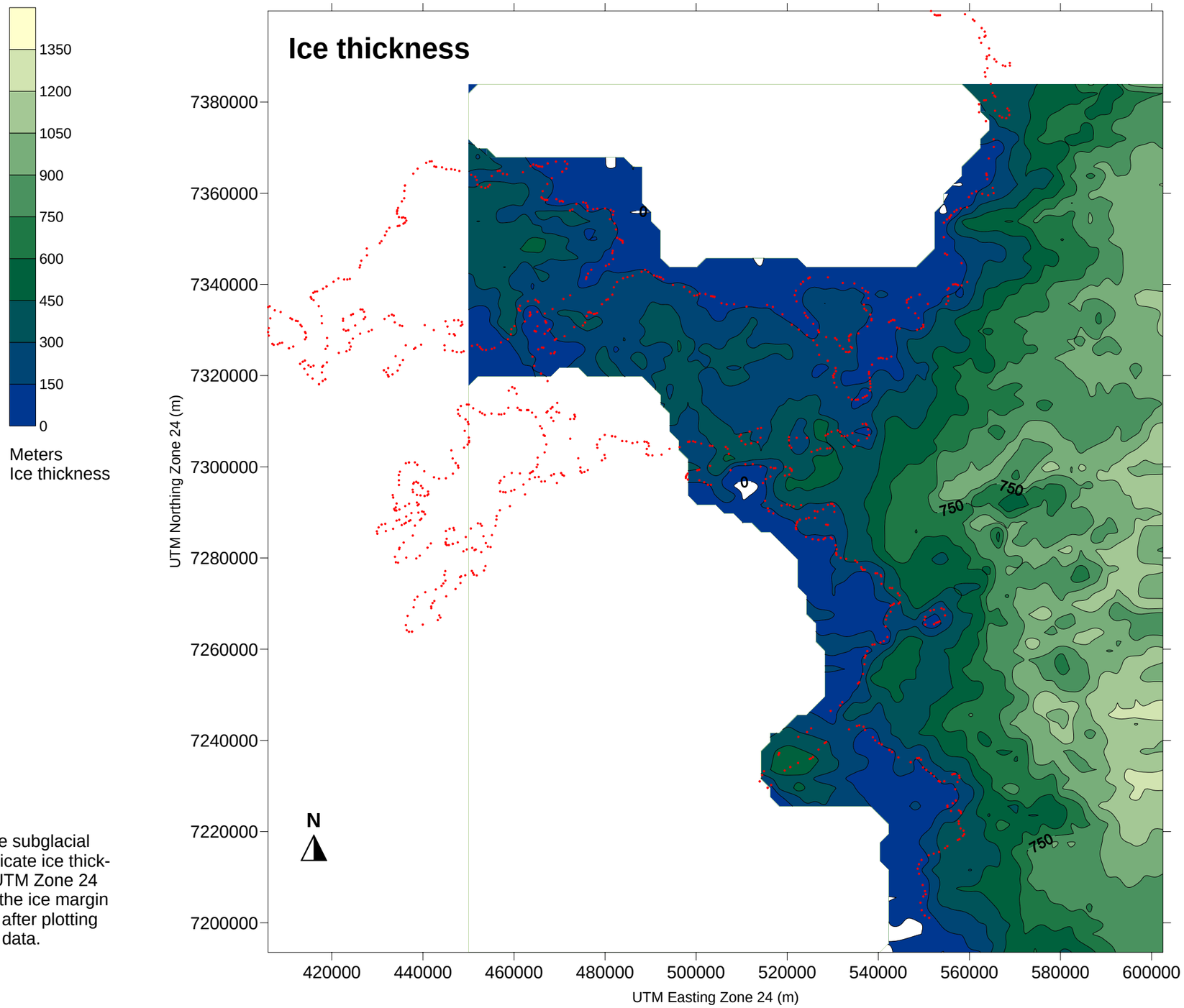

Figure 10 (enlarged version)

Map of the ice thickness derived from the subglacial and ice surface elevations. Contours indicate ice thickness in metres. The coordinates are in UTM Zone 24 projection. The red dotted line indicates the ice margin (see Section 2.2). The grid was blanked after plotting to exclude areas for which there was no data.